



# Seismic demand of the 2016–2017 Central Italy earthquakes

F. Mollaioli<sup>1</sup> · O. AlShawa<sup>1</sup> · L. Liberatore<sup>1</sup> · D. Liberatore<sup>1</sup> · L. Sorrentino<sup>1</sup>

Received: 6 April 2018 / Accepted: 7 August 2018 / Published online: 14 August 2018  
© Springer Nature B.V. 2018

## Abstract

The seismic sequence which started on August 24th, 2016, caused hundreds of casualties, damage and collapses in four regions of Central Italy (Lazio, Umbria, Abruzzo and Marche). The strongest event, which occurred on October 30th ( $M_w$  6.5), was forerun by four earthquakes with magnitude between 5.4 and 6.0. So far, a total of nine events with magnitude greater than or equal to 5.0 have taken place in the affected area. The earthquakes were caused by normal faults, all of them having NW–SE or NNW–SSE strike, approximately along the spine of the Apennine Mountains. The hypocentres of the events were at a shallow depth, between 8 and 10 km. The building stock in the affected area is mainly characterised by unreinforced masonry and reinforced concrete ordinary buildings, churches and historical constructions. Different municipalities, severely damaged, were not classified as seismic prone until 1981, or were originally attributed to a seismic zone with lower seismicity compared to the current one. This circumstance can explain, to a certain extent, the observed seismic response. In this study, aimed at interpreting the observed damage, the assessment of the damage potential of the ground motions recorded during the strongest events is performed by means of conventional and unconventional parameters. Specifically, elastic spectral demands, in terms of pseudo-accelerations, energies (equivalent velocity), displacements and rocking rotations are estimated, discussed and, whenever appropriate, compared with those of Italian seismic codes. Finally, different parameters related to the ground motion records destructiveness are calculated and compared with those obtained for other Italian earthquakes, highlighting how severe the 2016–2017 seismic sequence was.

**Keywords** Strong ground motion · Pseudo-acceleration · Energy · Displacement · Rocking · Intensity measures

## 1 Introduction

Between August, 2016, and January, 2017, nine events of magnitude greater than or equal to 5.0 struck the central part of Italy (Table 1). The first two events, which took place on August 24th, had  $M_w$  6.0 and 5.4, the third and the fourth ( $M_w$  5.4 and 5.9) occurred on October 26th,

---

✉ F. Mollaioli  
fabrizio.mollaioli@uniroma1.it

<sup>1</sup> Università degli Studi di Roma La Sapienza, Rome, Italy

**Table 1** 2016–2017 Central Italy seismic sequence

Id	Date, UTC	$M_w$	Epicentre	Depth (km)	Latitude °N	Longitude °E
<i>a</i>	2016-08-24, 02:36:32	6.0	1 km W of Accumoli (RI)	8	42.70	13.23
<i>b</i>	2016-08-24, 03:33:28	5.4	5 km E of Norcia (PG)	8	42.79	13.15
<i>c</i>	2016-10-26, 18:10:36	5.4	3 km SW of Castelsantangelo sul Nera (MC)	9	42.88	13.13
<i>d</i>	2016-10-26, 20:18:05	5.9	3 km NW of Castelsantangelo sul Nera (MC)	8	42.91	13.13
<i>e</i>	2016-10-30, 06:40:17	6.5	5 km NE of Norcia (PG)	9	42.83	13.11
<i>f</i>	2017-01-18, 09:25:40	5.1	3 km NE of Monteraie (AQ)	9	42.55	13.26
<i>g</i>	2017-01-18, 10:14:09	5.5	2 km W of Capitignano (AQ)	9	42.53	13.28
<i>h</i>	2017-01-18, 10:25:23	5.4	3 km S of Capitignano (AQ)	9	42.49	13.31
<i>i</i>	2017-01-18, 13:33:36	5.0	3 km N of Barette (AQ)	10	42.48	13.28

Events with moment magnitude greater than or equal to 5.0. Id labels are used in Fig. 1

the fifth ( $M_w$  6.5) on October 30th, and the other four on 18th January, 2017 ( $M_w$  5.1, 5.5, 5.4, and 5.0). The earthquake of October 30th ( $M_w$  6.5) was the strongest that occurred in Italy after the 1980 Irpinia earthquake ( $M_w$  6.9). The hypocentres of all events were at a shallow depth, approximately between 8 and 10 km.

The main events of the seismic sequence took place in a territory that was affected by relevant earthquakes in the past. Some of these earthquakes occurred within sequences, even though not equivalent to the present one. For example, the long and complex sequence of the year 1703, with two main events of magnitude 6.9 and 6.7, that had a much more widespread impact, occurred in the same area. The current earthquake sequence occurred in a gap between two earlier damaging events, namely, the 1997 Umbria-Marche seismic sequence to the NW and the 2009 L'Aquila earthquake to the SE. All the events occurred along the spine of the Apennine Mountain on a normal fault system, according to a NW–SE or NNW–SSE strike and dip approximately towards SW. The system is extended between Colfiorito and Campotosto and is potentially capable of earthquakes with magnitude up to 7.0.

The first event of August 24th caused severe damage to the municipalities of Amatrice, Arquata del Tronto and Accumoli, with 299 fatalities and several hundreds of people injured. The October events produced significant damage to the municipalities of Norcia and Castelsantangelo sul Nera, without additional fatalities (Tertulliani and Azzaro 2016). On the whole, Amatrice and Norcia can be considered representative of what was observed during the seismic sequence. Amatrice, which attracts a substantial touristic flow, suffered the highest toll of human lives, 229, due to a higher exposure for a famous festival scheduled for the end of the week of the first event, combined with the very poor performance of dwellings, whereas all the three heritage towers and a six-storey reinforced concrete building were damaged but did not collapse during the August events (Fig. 2a). The reinforced concrete building and the belfry of the towers collapsed at the end of October, and the bell tower of Sant'Agostino collapsed in January. Norcia, which is an important municipality in the affected area, was not significantly damaged by the August events. This circumstance could be attributed to its seismic history of the last centuries and, particularly, to its 1860 building code, as well as to repair and strengthening interventions made after the 1979 Norcia and, to a lesser extent, 1997 Umbria-Marche earthquakes (Sorrentino et al. 2017b). However, during the October events, almost all churches in Norcia suffered extremely severe damage (Fig. 2b). Such performances are certainly related to different buildings vulnerability (Borri et al. 2017), but are also a result of the specific demands of the ground motion as will be shown in the following sections.

In this study, the accelerograms recorded at a number of station have been investigated, focusing on their damage potential. To this aim, different Intensity Measures (IMs) have been estimated, and acceleration, energy, displacement and rocking spectra have been calculated and analysed in detail. However, due to the extremely large amount of information collected, only the most significant results are shown and discussed here. For this reason, different subsets of records have been used to discuss the different features of the earthquake sequence by considering the records with the highest demands of the corresponding IMs.

## 2 Records

The seismic sequence was recorded by the permanent and temporary stations of the Italian National Seismic Network, managed by the Italian National Institute of Geophysics and Volcanology, as well as by the Italian National Accelerometric Network, managed by the

Department of Civil Protection. The records of all events are collected in the Engineering Strong Motion database (Luzi et al. 2017).

In this study, stations that recorded the nine events reported in Table 1 and that are placed within about 40 km from the respective epicentres are considered. Those stations whose records have been explicitly discussed are listed in Table 2, together with their geographical coordinates and site classification, according to the Italian Building Standard (DMIT 2018). It should be noted that the station of Forca Canapine (FCC) is not included in the present study, although it recorded high value of Peak Ground Acceleration (PGA), because it is currently under revision.

In Fig. 1 there are shown the epicentres of the events, the recording stations considered, and the surface projection of the faults of the three events with the largest magnitude (Tinti et al. 2016; Chiaraluce et al. 2017).

### 3 Intensity measures

Table 3 shows the selected intensity measures (IMs) of the horizontal components considered in this study. With the aim of comparison, the same IMs have been estimated for other Italian earthquakes. In addition to classical instrumental PGA and peak ground velocity (PGV), other parameters useful in the interpretation of the damage potential of ground motion have been considered:

- Maximum incremental velocity (IV), given by the area enclosed by the largest acceleration pulse (Anderson and Bertero 1987).
- Housner intensity ( $I_H$ ), defined as the area below the elastic pseudo-velocity spectrum between the periods of 0.1 s and 2.5 s:

**Table 2** Strong motion stations of Central Italy earthquakes of 2016–2017, explicitly mentioned in this study (Fig. 1)

ID	Station	Latitude °N	Longitude °E	Station name	Site class
1	CMI	42.850	13.093	Campi	C <sup>a</sup>
2	NRC	42.793	13.096	Norcia	B
3	CNE	42.894	13.153	Castelsantangelo Sul Nera	C <sup>a</sup>
4	NOR	42.792	13.092	Norcia Le Castellina	B
5	ACC	42.696	13.242	Accumoli	A <sup>a</sup>
6	TI201	42.657	13.251	Domo	B <sup>a</sup>
7	AMT	42.632	13.286	Amatrice	B
8	CLF	43.037	12.920	Colfiorito	D
9	FOC	43.026	12.897	Foligno-Colfiorito	C <sup>a</sup>
10	PCB	42.558	13.338	Poggio Cancelli (Base Diga)	B <sup>a</sup>
11	MSC	42.527	13.351	Mascioni (Campotosto)	B <sup>a</sup>
12	MSCT	42.527	13.351	Mascioni	B <sup>a</sup>
13	NCR	43.112	12.785	Nocera Umbra	E
14	CLO	42.829	13.206	Castelluccio di Norcia	A <sup>a</sup>
15	TI213	42.725	13.126	Savelli PG	A <sup>a</sup>

<sup>a</sup>Site classification is not based on a direct  $V_{s,30}$  (average shear wave velocity in the top 30 m) measurement

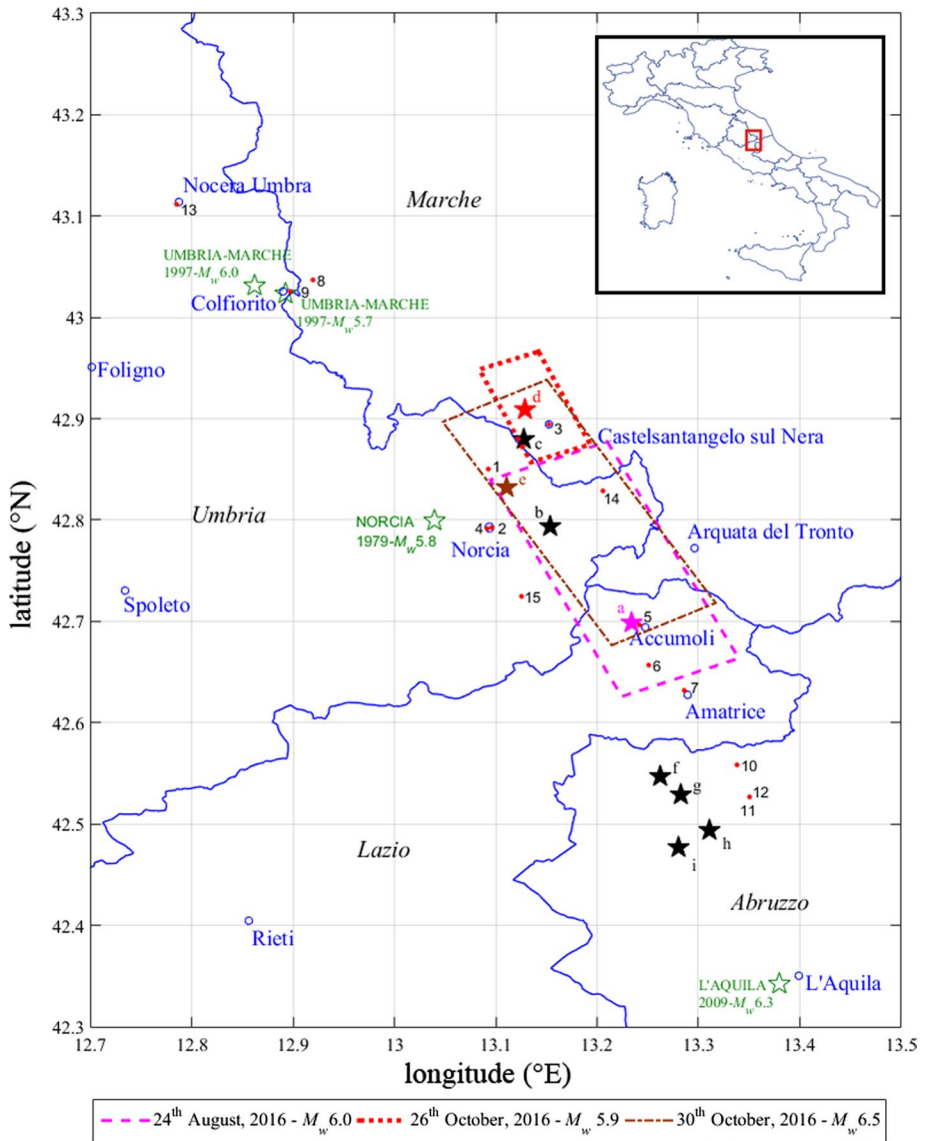


**Fig. 1** Investigated area. Epicentres of the earthquakes listed in Table 1 (solid stars); surface projection of the faults of the most severe events; accelerometer stations (dots, numbers refer to the station listed in Table 2). Empty stars represent the epicentres of previous earthquakes

$I_H = \int_{0.1}^{2.5} S_{pv}(T, \xi = 0.05) dT = \frac{1}{2\pi} \int_{0.1}^{2.5} S_{pa}(T, \xi = 0.05) T dT$ ; where  $S_{pv}$  is the pseudo-velocity at the undamped natural period  $T$  and damping ratio  $\xi = 0.05$ , and  $S_{pa}$  is the pseudo-acceleration at the undamped natural period  $T$  and damping ratio  $\xi = 0.05$  (Housner 1952). Housner intensity can also be considered as the first moment of the area of  $S_{pa}$  ( $0.1 \text{ s} \leq T \leq 2.5 \text{ s}$ ) about the  $S_{pa}$  axis. This implies that it is larger for

**Table 3** Intensity measures of horizontal components of selected records

Station name	Location	Site class	$D_e$ (km)	$D_f$ (km)	PGA (g)	PGV (cm/s)	IV (cm/s)	$I_H$ (cm)	EPA (g)	$t_D$ (s)	$I_A$ (cm/s)
24th August, 2016— $M_w$ 6.0											
AMT_E	Amatrice	B	8.9	1.4	<b>0.87</b>	<b>43.6</b>	<b>62.9</b>	75.1	<b>0.61</b>	3.7	<b>187.9</b>
AMT_N	Amatrice	B	8.9	1.4	0.38	41.5	58.9	<b>112.9</b>	0.29	3.2	72.0
NRC_E	Norcia	B	13.7	2.0	0.36	29.8	48.1	107.0	0.31	6.0	104.2
NRC_N	Norcia	B	13.7	2.0	0.37	23.7	28.9	80.1	0.30	6.3	82.3
26th October, 2016— $M_w$ 5.4											
CMI_E	Campi	C*	4.4	—	<b>0.72</b>	<b>55.7</b>	<b>95.5</b>	<b>129.9</b>	<b>0.60</b>	2.6	<b>242.9</b>
CMI_N	Campi	C*	4.4	—	0.34	18.6	32.7	40.5	0.27	4.6	59.9
CNE_E	Castelsantangelo sul Nera	C*	2.6	—	0.56	17.3	28.8	33.5	0.35	3.9	117.6
FOC_E	Foligno Colfiorito	C*	25.3	—	0.34	13.0	21.5	15.8	0.23	3.9	49.6
NOR_E	Norcia	B	9.8	—	0.16	21.7	42.2	75.1	0.12	<b>8.8</b>	24.1
NRC_E	Norcia	B	10.3	—	0.30	25.8	27.6	65.0	0.21	5.6	36.5
26th October, 2016— $M_w$ 5.9											
CMI_E	Campi	C*	7.1	3.5	<b>0.65</b>	<b>43.8</b>	<b>69.4</b>	<b>141.6</b>	<b>0.60</b>	5.3	227.0
CMI_N	Campi	C*	7.1	3.5	0.31	25.9	34.2	62.7	0.29	7.8	98.6
CNE_E	Castelsantangelo sul Nera	C*	3.1	0.0	0.54	23.1	37.4	79.2	0.39	4.5	116.2
CNE_N	Castelsantangelo sul Nera	C*	3.1	0.0	0.38	36.5	48.9	98.3	0.32	5.2	102.0
FOC_E	Foligno Colfiorito	C*	23.0	17.5	0.62	20.0	39.6	31.5	0.45	5.2	201.8
NOR_E	Norcia	B	13.3	8.0	0.22	20.9	30.3	62.6	0.16	<b>17.3</b>	27.6
NRC_E	Norcia	B	13.9	7.8	0.25	16.2	27.6	51.3	0.16	11.8	30.4
30th October, 2016— $M_w$ 6.5											
ACC_E	Accumoli	A*	19.4	0.0	0.43	44.1	74.1	140.3	0.39	5.5	200.5
AMT_E	Amatrice	B	27.2	7.1	0.53	37.9	50.9	89.8	0.40	5.3	155.5
NOR_E	Norcia	B	4.9	2.5	0.31	56.3	94.0	<b>253.8</b>	0.26	<b>15.1</b>	288.7
NRC_E	Norcia	B	5.4	2.2	0.49	48.3	84.5	203.4	0.46	10.4	362.4

**Table 3** (continued)

Station name	Location	Site class	$D_e$ (km)	$D_f$ (km)	PGA (g)	PGV (cm/s)	IV (cm/s)	$I_H$ (cm)	EPA (g)	$t_D$ (s)	$I_A$ (cm/s)
T1201_N	Domo	B*	23.3	3.3	0.48	<b>83.0</b>	<b>123.7</b>	212.7	0.35	4.6	223.6
CLO_E	Castelluccio di Norcia	A*	7.8	3.7	0.43	52.2	94.6	234.7	0.33	9.6	245.4
CLO_N	Castelluccio di Norcia	A*	7.8	3.7	0.58	66.1	102.7	203.7	0.50	9.1	422.3
T1213_E	Savelli PG	A*	12	0.0	<b>0.79</b>	60.7	89.5	152.1	<b>0.60</b>	6.5	<b>602.4</b>
18th January, 2017— $M_w$ 5.5											
AMT_E	Amatrice	B	11.5	—	0.31	16.1	23.5	31.9	0.23	2.9	34.8
AMT_N	Amatrice	B	11.5	—	0.33	15.8	25.8	43.6	0.24	2.2	36.8
MSCT_N	Mascioni (Campotosto) 2	B*	5.6	—	0.27	16.5	26.0	31.4	0.21	<b>3.9</b>	36.2
MSC_N	Mascioni (Campotosto)	B*	5.6	—	0.25	15.7	25.1	30.2	0.20	<b>3.9</b>	32.7
PCB_E	Poggio Cancelli	B*	5.6	—	0.41	16.9	29.3	40.7	0.35	2.6	94.2
PCB_N	Poggio Cancelli	B*	5.6	—	<b>0.59</b>	<b>21.0</b>	<b>35.0</b>	<b>48.3</b>	<b>0.48</b>	2.2	<b>193.5</b>
18th January, 2017— $M_w$ 5.4											
AMT_E	Amatrice	B	15.5	—	0.16	10.2	15.7	19.9	0.14	3.7	15.0
AMT_N	Amatrice	B	15.5	—	0.17	9.2	10.5	18.4	0.09	<b>4.2</b>	5.9
MSCT_E	Mascioni (Campotosto) 2	B*	4.9	—	0.23	17.0	23.8	<b>50.0</b>	0.16	4.0	26.5
MSC_E	Mascioni (Campotosto)	B*	4.9	—	0.21	16.1	22.5	47.7	0.15	4.0	23.0
PCB_E	Poggio Cancelli	B*	7.4	—	0.39	11.8	22.5	35.7	0.21	4.1	45.2
PCB_N	Poggio Cancelli	B*	7.4	—	<b>0.56</b>	<b>19.3</b>	<b>36.0</b>	46.3	<b>0.37</b>	3.8	<b>120.0</b>

Boldface values for event maximum values

$D_e$ , epicentral distance;  $D_f$ , distance between the recording station and the surface projection of the fault; PGA, peak ground acceleration; PGV, peak ground velocity; IV, maximum incremental velocity;  $I_A$ , arias intensity;  $t_D$ , Trifunac and Brady duration;  $I_H$ , Housner intensity; EPA, effective peak acceleration

\*Inferred from different geological and geotechnical sources



**Fig. 2** **a** Amatrice, after the August 24th event. Extensive damage and collapses in ordinary unreinforced masonry buildings and damage without collapses in tall buildings: six-storey reinforced concrete building, on the left, and Clock Tower from Corso Umberto I. **b** Part of the historical centre of Norcia after the October 30th event in the snapshot of a movie released by the Corps of Firefighters ([www.vigilfuoco.tv](http://www.vigilfuoco.tv)). Limited damage to ordinary unreinforced masonry buildings and extensive collapses to churches: (1) Santa Rita, (2) San Francesco, (3) Santa Maria Argentea, (4) San Benedetto and (5) San Filippo

ground motions with a significant amount of low frequency content. Dimensionally, Housner intensity is a displacement.

- Effective peak acceleration EPA (ATC 1978), given by the mean pseudo-acceleration,  $S_{pa,m}$ , in the period range 0.1–0.5 s, divided by 2.5 ( $EPA = S_{pa,m}/2.5$ ). The empirical constant 2.5 is essentially an amplification factor of the response spectrum obtained from real peak value records. If the ground motion consists of high frequency components, that generally have little effect on the seismic responses of structures, EPA will be obviously smaller than the actual peak value.
- Trifunac and Brady strong motion duration ( $t_D$ ):  $t_D = t_{0.95} - t_{0.05}$ ; where  $t_{0.05}$  and  $t_{0.95}$  are the time values at which the 5% and 95% of the time integral of the history of squared accelerations are reached, respectively (Trifunac and Brady 1975).
- Arias intensity ( $I_A$ ), which represents the sum of the total energies, per unit mass, stored at the end of the earthquake ground motion, in a population of undamped linear oscillators (Arias 1970):  $I_A = \frac{\pi}{2g} \int_0^{t_0} a_g^2(t) dt$ . Arias intensity, that dimensionally is a velocity, can be correlated to the damage (Cabañas et al. 1997) but tends to overestimate the intensity of an earthquake with long duration, high acceleration and broad band frequency content (Uang and Bertero 1988).

The highest PGA values for the most significant six events of the sequence are boldface in Table 3. They were recorded in Amatrice, Campi, Savelli and Poggio Cancelli. These values, which range between 0.56 and 0.87 g, have been hardly reached in Italy during other recent events. Only the ANR\_N record of the 1972 Ancona event ( $M_L$  4.7), the GMN\_E record of the September 1976 Friuli event ( $M_w$  5.9), the NCR\_E record of the 1997 Umbria-Marche event ( $M_w$  6.0) and the AQP records of the 2009 L'Aquila earthquake ( $M_w$  6.3) show comparable values.

Compared to the PGA, the velocity-based parameters provide a better approach to the definition of the destructive potential of earthquakes (Decanini et al. 2012). The highest PGV values (boldface in Table 3), measured in Amatrice, Campi, Norcia, Domo, Castelluccio di Norcia and Savelli range between 43.6 and 83.0 cm/s. Looking at previous Italian earthquakes, the largest PGV values recorded on Italian territory are related to the September 1976 Friuli event ( $M_w$  5.9), where a PGV of 68.4 cm/s was measured (GMN\_E



record), to the 1980 Irpinia earthquake ( $M_w$  6.9), where a PGV of 70 cm/s was measured (Sturno\_E record) and to the 2012 Emilia earthquake ( $M_w$  6.0), where a PGV of 57.5 cm/s was recorded (Mirandola, MRN\_N record).

Some interesting points arise when looking at the IV and  $I_H$  parameters. The largest values were found for the stations located in the near fault areas. Particularly, for the October 30th event it is possible to observe the highest values ever recorded in Italy: IV = 94 cm/s and  $I_H$  = 253.8 cm for NOR\_E record; IV = 84.5 cm/s and  $I_H$  = 203.4 cm for NRC\_E record; IV = 123.7 cm/s and  $I_H$  = 212.7 cm for T1201 record; and IV = 94.6 cm/s and  $I_H$  = 234.7 cm for CLO\_E record. High values of  $I_H$ , as already mentioned, indicate that the acceleration spectrum is shifted towards low frequencies, as will be highlighted by acceleration and energy spectra. This is also an index of the presence of long duration pulses due to directivity or soil amplification effects. Considering the extremely good correlation between damage to churches and  $I_H$  (Marotta et al. 2017b), as well as the sensitivity of local mechanisms to long period pulses (Sorrentino et al. 2014), systematic damage to churches in Norcia after the October 30th event (Fig. 2b) can find some explanation. In addition, the comparison between PGA and EPA values highlights the presence of high frequency components. For example, it is possible to observe for the records AMT\_E (August 24th,  $M_w$  6.0), CMI\_E (October 26th,  $M_w$  5.4), CMI\_E (October 26th,  $M_w$  5.9), and T1213 (October 30th,  $M_w$  6.5) the same EPA value (0.6 g) but different PGA values, i.e. 0.87 g, 0.72 g, and 0.65 g, and 0.79 g, respectively. It is also noted that EPA values in the 2016–2017 sequence are larger than the largest value measured in Italian past earthquakes, which is equal to 0.51 g (Nocera Umbra NS record, 1997 Umbria-Marche earthquake,  $M_w$  6.0).

As far as the effective duration of the motion is concerned, the Trifunac and Brady duration,  $t_D$ , is in the range 1.2–20.4 s for the whole database. These values show that the significant phase of the motion was quite short. However, the duration alone cannot be considered a suitable index for the characterisation of the damage potential because in some cases, due to directivity effects, high destructive capacity of the ground motion corresponds to a short effective duration (Mollaioli et al. 2006). The effective duration depends also on the soil type under the recording instruments and the magnitude of the event. The largest Arias Intensity value,  $I_A$ , equal to 602.4 cm/s, was achieved for the T1213\_N record (October 30th,  $M_w$  6.5). However, for this record it is possible to note a prominent high-frequency content with maximum spectral amplification in the range of periods between 0.00 and 0.25 s.

## 4 Conventional linear-elastic damped spectra

### 4.1 Pseudo-acceleration spectra of the horizontal components

In Fig. 3, the 5% damped elastic pseudo-acceleration spectra are shown for the horizontal components of the six events of the seismic sequence with largest ordinates (Table 3). Peak values of the August 24th event occur in the range of period 0.1–0.5 s with a fast decrease for higher periods. The fundamental period of vibration of ordinary unreinforced masonry and reinforced concrete buildings can be estimated using the simplified formula in the Italian building standard (DMIT 2018), which depends only on material and building height. Typical height of unreinforced masonry buildings in the historical centre of Amatrice was about 10–12 m (Fumagalli et al. 2017), resulting in a fundamental period of about 0.3 s. The six-storey reinforced building that survived the August event results in a period more

than double (Fig. 2a). A similar value can be estimated for the Clock Tower, based on the formula suggested by Curti et al. (2012). The AMT station is located about 400 m from the Clock Tower and there is a difference of altitude of about 70 m, therefore the actual shaking in Amatrice historical centre is unknown. Nonetheless, there is some indication that seismic demand has been rather severe on ordinary unreinforced masonry buildings and somewhat more limited on taller structures.

Prevalence of high demand in the low periods range is observed also in all other events, with the exception of the October 30th one, which exhibits a richest frequency content with secondary peaks at longer periods. For this event, values of spectral acceleration exceeding 1.0 g are detected also for periods around 1.0 s, for both Norcia stations despite the different position (about 400 m distance) and NOR station being housed within a massive structure. Such high demands for medium-long periods can explain the extensive damage to churches observed in Norcia (Fig. 2b), considering the sensitivity of their local mechanisms to low frequencies (Marotta et al. 2017b).

Maximum values of spectral acceleration are close, or even greater than 2.0 g. Such values are higher than the spectral accelerations of recent events occurred in the Central Apennine area (Decanini et al. 2000, 2012).

### 4.2 Comparison with Italian seismic codes

It is important to highlight that the wide majority, if not the entirety, of collapses or severe damage in recent earthquakes involved buildings not complying with the requirements of current seismic codes. Therefore, in order to understand the relation between the observed

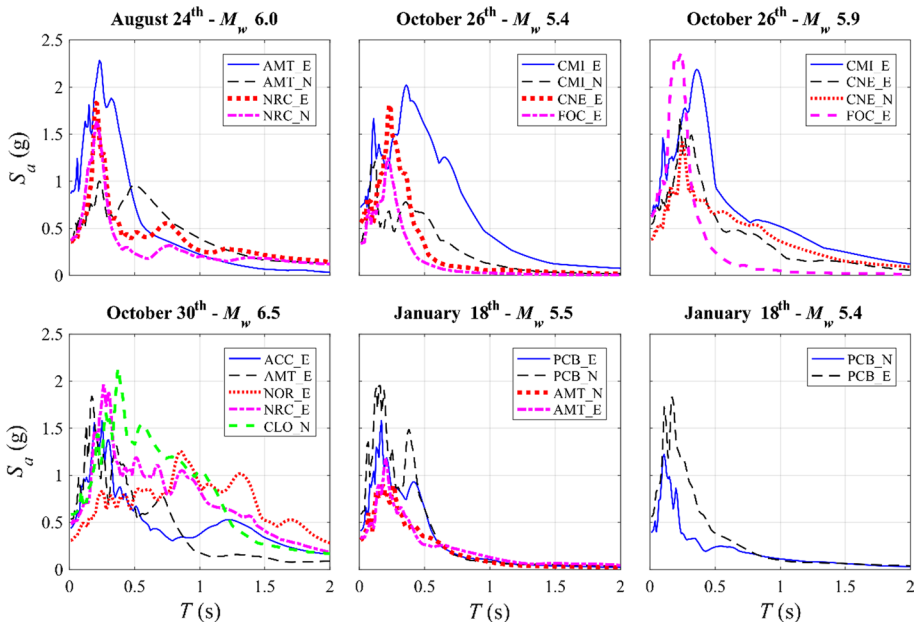


Fig. 3 Largest pseudo-acceleration spectra for the six main events of the sequence

damage scenario and the intensity of the seismic sequence, it is important to look at the updating of the seismic classification and seismic code.

The evolution of the Italian Seismic Code was characterized by various discontinuities since its first introduction (Sorrentino 2007). An outline is presented in Table 4. Major modifications date back to 1975 (DMLP 1975), when the response spectrum was introduced for the first time, and to 1996 (DMLP 1996), when the limit state method was included, as alternative to the allowable stress method. Due to the introduction of additional coefficients to be used within the limit state procedure (DMLP 1996), the comparison between design spectra prescribed before and after 1996 is possible only by multiplying the seismic lateral coefficient of the former by a factor depending on the material (e.g. 2.25 for concrete) and a coefficient to convert the design spectrum into an elastic one (behaviour factor). For example, with reference to a seismic coefficient of 0.07 (year 1962 in Table 4) and assuming a behavior factor of 4, the plateau of the elastic design spectrum for seismic zone 2, is equal to 0.63 g for concrete structures (Decanini et al. 2012). Another important changes occurred in 2003, with the introduction of the capacity design method (OPCM 2003). This updating process brought to the release of a comprehensive building code in 2008 (DMI 2008), which has been recently revised (DMIT 2018).

The seismic classification has also been updated several times in the last century. From the 1908 Messina and Southern Calabria earthquake to 1974, municipalities were classified as seismic prone and subjected to rigorous standards for construction only after being severely damaged by earthquakes. In some cases, there has been a declassification under local pressure to deregulate construction business. In 1981, it was proposed to classify the national territory in three seismic zones, which, however, covered only half of the country. After the 2002 Molise earthquake, the whole country was reclassified in four seismic zones (OPCM 2003). Finally, since 2008 (DMI 2008), the expected maximum acceleration at the site is no longer defined by dividing the territory

**Table 4** Evolution of the Italian seismic code, main changes throughout the last century

Year	Major code changes
1909	One seismic zone (small part of the Italian territory) with seismic coefficient equal to 1/8 or 1/6, depending on the building height. Prescriptions about building dimensions and distances
1927	Introduction of the second seismic zone, in which the prescribed seismic coefficient is 1/10 or 1/8, depending on the building height
1937	Seismic coefficient equal to 0.10 and 0.05 in seismic zones 1 and 2, respectively
1962	Seismic coefficient in seismic zone 2 increased to 0.07
1975	Introduction of the response spectrum, constant values (same values of the seismic coefficient as in 1962) up to 0.8 s and decreasing hyperbolic curve for higher periods
1984–1986	Introduction of the third seismic zone, significant increment of the number of municipalities classified as seismic prone. Spectral ordinates at low periods (0.0–0.8 s) equal to 0.10, 0.07 and 0.04 g in zone 1, 2 and 3, respectively
1996	Introduction of the limit state method, as alternative to the allowable stress method (both methods were permitted)
2003	Introduction of a fourth seismic zone. The whole territory is included in the seismic classification. Introduction of the capacity design method. Spectrum shape derived from EuroCode 8
2008	Comprehensive Building Code. Site specific peak ground and spectral accelerations defined for different probability of exceedance
2018	Revision of the 2008 Building Code. Response spectra are the same as in the 2008 code

in seismic zones, but as a function of geographic coordinates of the site, return period and different percentiles of the spectral ordinates confidence level (16th, 50th and 84th).

Considering the municipalities affected by the earthquake sequence, the following observations can be made:

- Several municipalities of the epicentral areas were classified as seismic prone only during the 1980s. For example Nocera Umbra and Foligno (Umbria region) were classified in 1981, whereas the municipalities in the Marche region, e.g. Ussita, Visso and Arquata del Tronto, were classified in 1983. The majority of the damaged buildings were constructed before and, consequently, designed without any seismic prescription.
- To some municipalities classified before the 1980s (e.g. Accumoli and Amatrice) a lower than current seismic hazard was attributed;
- For the municipalities classified before the 1980s no spectrum was used until 1975.

Finally, a particular attention should be devoted to Norcia, classified in the highest seismicity zone until 2008, when the seismic zones were replaced by the current approach. After the 1859 earthquake, the buildings were reconstructed with a limited number of storeys and specific details to improve earthquake performance (Sorrentino et al. 2017b). Moreover, Norcia was subjected, in 1979, to an earthquake with Mercalli-Cancani-Sieberg (MCS) intensity VIII, with source-to-site distances ranging from 15 to 20 km. Subsequently, buildings were repaired and reinforced. After the 1997 Umbria-Marche seismic sequence some damage was observed and new interventions were applied. Therefore, a large part of the building stock in Norcia was strengthened (Sisti et al. 2018).

In Fig. 4 the pseudo-acceleration response spectra associated to the most severe horizontal ground motions recorded during the 24th August and 30th October events by the stations of Amatrice (AMT) and Norcia (NRC) are compared with the elastic spectra provided by the Italian seismic code (DMIT 2018) at the corresponding sites for soil class B and three different return periods  $T_R=475, 975$  and  $2475$  years, corresponding to probabilities of exceedance in 50 years equal to 10%, 5% and 2%, respectively. The comparison of individual records with code spectra is a delicate task (Crowley et al. 2009; Iervolino 2013) due to a number of reasons, the first of which being the probabilistic nature of the latter, which are based on uniform hazard spectra (Stucchi et al. 2011). Nonetheless, some valuable results can be highlighted by such a comparison. In the same figure, the spectrum of the 1996 Italian Code (DMLP 1996) is also shown.

First of all, it is possible to observe that the AMT\_E spectra largely exceed, in the plateau range of periods, the 2475 year return period spectrum. A similar circumstance is detected for the Norcia records (NRC) of August 24th and October 30th. Moreover, for the NRC\_E component, and, to a lesser extent, for the NRC\_N component, of the October 30th event, it is also observed the presence of secondary peaks exceeding all the design spectra for vibration periods between about 0.7 and 1.5 s (Fig. 4b). This occurrence suggests the possible presence of pulses due to forward directivity effects (see also Sect. 5), even though Bindi et al. (2011) highlighted that the Norcia sites are affected by strong amplifications in the frequency range 0.5–5 Hz due to the particular soil characteristic. To identify the presence of pulses, further analyses have been then performed using Baker's method (2007), the variational mode decomposition technique (Dragomiretskiy and Zosso 2014) and the approach suggested by Zhai et al. (2013), also reported in Chang et al. (2016). Such analyses clearly identified the presence of pulses, although they cannot be directly related to the physical rupture process.

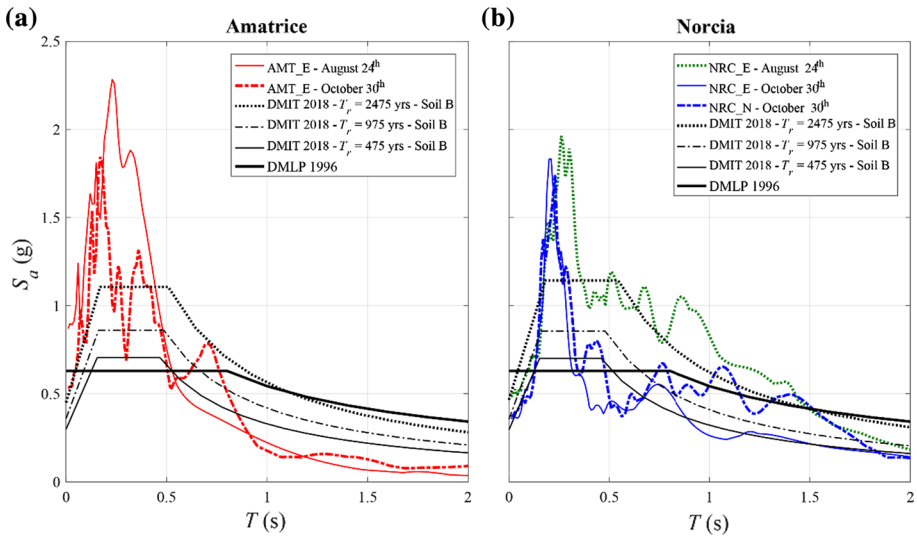


**Fig. 4** Largest pseudo-acceleration response spectra of the horizontal ground motions recorded during the August 24th and October 30th events compared to the elastic spectra provided by current (DMIT 2018) and mid 1990s (DMLP 1996) Italian seismic codes. Stations of: **a** Amatrice (AMT) and **b** Norcia (NRC)

### 4.3 Vertical component

The acceleration spectra of the vertical component of the August 24th and October 30th events are shown in Fig. 5. The spectra are grouped according to the distance between the recording station and the surface projection of the fault,  $D_f$ . For the October 30th event, mean spectra are also shown. The vertical spectral accelerations are significant, especially in the near fault. Peak values are generally attained in the period range 0.00–0.35 s. Nevertheless, in some cases large vertical spectral accelerations are observed at longer periods. For example, with reference to the August 24th event, the AMT spectrum (Amatrice station) exhibits vertical acceleration of about 0.5 g at 0.5 s. Considering the October 30th event, the CLO spectrum shows two peaks: the first one at 0.2 s (2.20 g) and the second one at 0.45 s (1.26 g). The same trends are observed in several stations for different events of the sequence.

Vertical elastic code spectra in Amatrice for three return periods, i.e. 475, 975 and 2475 years, are depicted in Fig. 5 as well. Code spectra in Norcia are almost the same as those in Amatrice, due to the proximity of the two locations to one another. Considering the near fault records ( $D_f < 5$  km), the event of October 30th appears extremely severe, with the mean spectral values significantly higher than those of the code spectra for the return period of 2475 years. For the stations with distances  $D_f$  in the distance range 5–12 km, the mean spectra approximate fairly well the 2475 years return period code spectrum. With reference to the August 24th event, for some records the spectral accelerations in the period range 0.5–1.0 s exceeds the median elastic code spectra.

Finally, although not shown herein for the sake of conciseness, the most severe vertical acceleration spectra of the Central Italy earthquake have been compared to those of the 2009 L'Aquila earthquake (Decanini et al. 2012) and the 2012 Emilia event, where the effect of the vertical component was significant (Liberatore et al. 2013). These other records exhibit

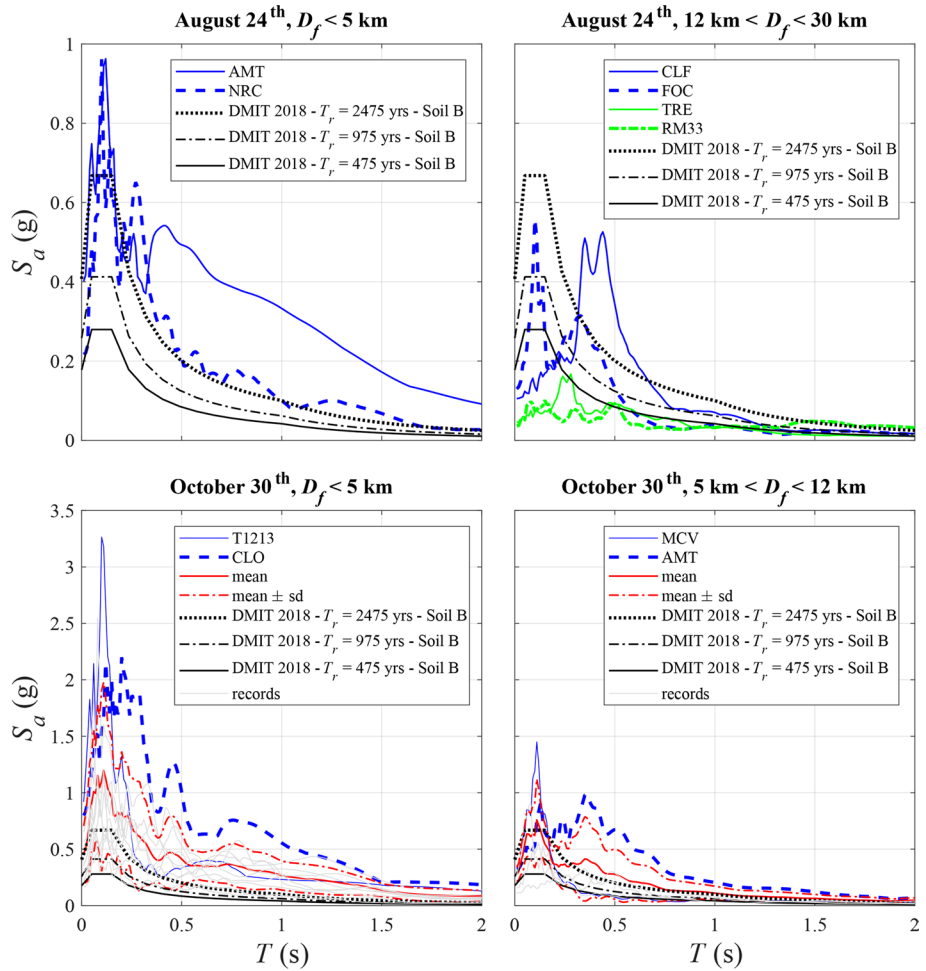


**Fig. 5** Vertical acceleration spectra grouped according to the distance to the fault. Code spectra (DMIT 2018) related to Amatrice

considerable vertical spectral accelerations at periods less than or equal to 0.1 s. The Central Italy record CLO is shifted towards higher periods, showing to be the most severe for periods greater than 0.15 s. In this period range, due to the simultaneous presence of a high horizontal seismic demand, the presence of the vertical component may negatively affect the response of framed structures, due to the variation of the axial force in the columns and the consequent reduction of their shear capacity (Decanini et al. 2002; Shrestha 2009).

### 5 Energy spectra (equivalent velocity)

Various approaches to seismic design beyond the traditional force-based procedures in the context of Performance Based Seismic Design were proposed. These include the displacement-based design methods and the energy-based formulations. Energy-based procedures, wherein the energy imparted to the structure by the earthquake is balanced by providing adequate energy dissipation capacity, can also form the basis of estimating expected seismic demands, assessing in this way the destructive potential of earthquake ground motions. Two different input energies can be considered for a single degree of freedom system (Uang and Bertero 1990): the absolute input energy,  $E_{Ia} = \int_0^t m \ddot{u}_a du_g$ , and the relative input energy,  $E_{Ir} = \int_0^t m \ddot{u}_r du_g$ , where  $m$  is the mass of the oscillator,  $\ddot{u}_a$  and  $\ddot{u}_r$  are the absolute and relative accelerations, respectively, and  $u_g$  is the ground displacement. These two energy parameters can be converted into equivalent velocities using the following relations:  $V_{Ela} = \sqrt{2E_{Ia}/m}$  and  $V_{Elr} = \sqrt{2E_{Ir}/m}$ .

In the following, for the sake of brevity, only the case of absolute input energy is discussed. In Figs. 6 and 7, a comparison is shown between elastic input energy design spectra proposed by Decanini and Mollaioli (1998) and the input energy spectra of significant records of the 2016 seismic sequence as well as the largest input energy spectra ever obtained in recorded Italian earthquakes.

Decanini and Mollaioli design spectra, here presented for soil classes S1 and S2 corresponding approximately to A and B, C classes of the Italian building code (DMIT 2018), are defined to match the mean plus a standard deviation of a set of about 300 accelerograms. These figures highlight the severe damage potential of some records of the sequence. The NOR\_E and NRC\_E, roughly oriented according to the fault-normal direction in the near fault area, present distinct peaks in the range of periods between 0.85 and 1.50 s, which approximately correspond to the durations of the forward directivity pulses (Mollaioli and Bosi 2012). Particularly, NOR\_E exceeds the design spectra, even though only close to its maximum value, which exceeds  $72,000 \text{ cm}^2/\text{s}^2$  and is the highest ever recorded in Italy. Thus, it is confirmed that, for near fault records, maximum energy demands shift towards low frequencies with increasing magnitude (Mollaioli and Bosi 2012). The high energy demand,  $E_{I,max} = 21,935 \text{ cm}^2/\text{s}^2$ , for the CMI\_E component of the  $M_w$  5.4 October 26th event, is the highest value observed in Italy for low magnitude events

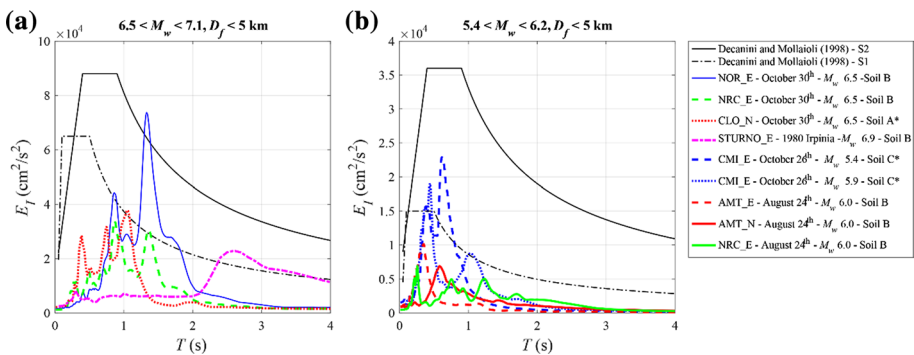


**Fig. 6** Comparison with elastic input energy design spectra proposed in Decanini and Mollaioli (1998). **a**  $6.5 < M_w < 7.1$ , distance  $D_f < 5 \text{ km}$ , soil S1 and S2. Sturmo spectrum of the 1980 Irpinia earthquake ( $M_w$  6.9) is also shown and **b**  $5.4 < M_w < 6.2$ , distance  $D_f < 5 \text{ km}$ , soil S1 and S2

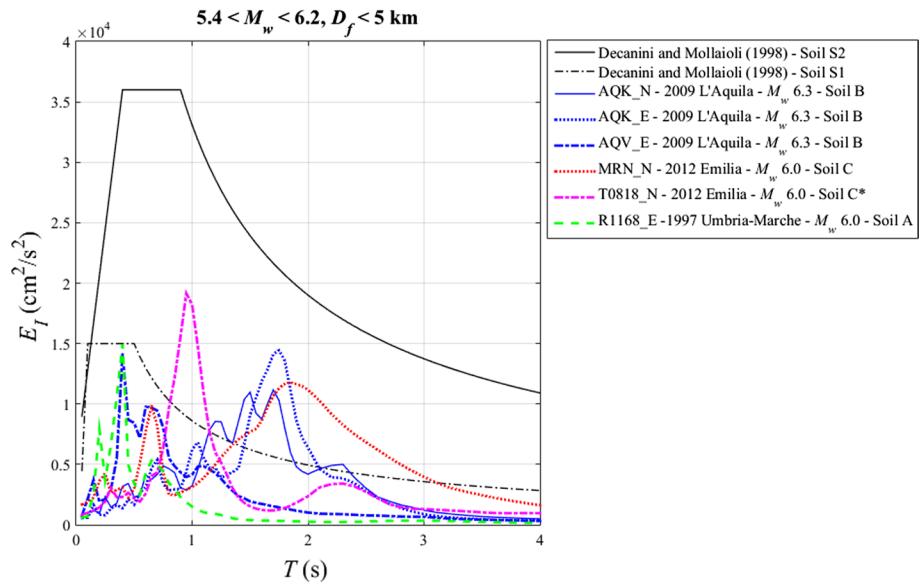


**Fig. 7** Comparison of elastic input energy design spectra proposed in Decanini and Mollaioli (1998) with input energy spectra of records obtained during the 2009 L'Aquila earthquake (AQK\_N, AQK\_E, AQV\_E), the 2012 Emilia earthquake (MRN\_N and T0818\_N), and the 1997 Umbria-Marche earthquake (R1168\_E)

(Fig. 6b). This value is also comparable, in the same range of periods, with the maximum energy demand of the T0818\_N component ( $E_{I,max} = 19,153 \text{ cm}^2/\text{s}^2$ ) recorded during the 2012 Emilia earthquake on soil C (Fig. 7).

The severity of the two strongest events of the sequence in the near fault region can also be appreciated in Fig. 8, where the AMT components (August 24th event) and the NOR\_E and NRC\_E components (October 30th event) are compared with the spectra obtained from recent proposed ground motion prediction equations of elastic input energy equivalent velocity (Cheng et al. 2014). Mainly, while for the case of AMT the highest demand is concentrated in the high-frequency range, the predicted spectra are significantly exceeded by the NOR\_E and NRC\_E spectra in the medium-period range (between 0.85 and 2.00 s).

It was observed that the dynamic characteristics of ground shaking can significantly differ as a function of the location of the recording station with respect to the fault and the evolution of the rupture process, particularly when the recording station is placed in the near fault area. It is well known that, under certain conditions, earthquake ground motions can consist of a limited number of distinct velocity medium-to-long duration pulses. Such impulsive characteristic of near-source ground motions reflects on the maximum energy demand (Mollaioli et al. 2006, 2011; Mollaioli and Bosi 2012). Moreover, the period corresponding to the energy peak in the medium-to-long duration range is strictly correlated with the pulse duration (Mollaioli and Bosi 2012; Mollaioli et al. 2014).

The parameters of the finite-fault geometries shown in Fig. 1 permit to infer that the pulse-like features of some records could be due to forward directivity effect. The August 24th event shows substantially a bilateral rupture that started below the town of Accumoli toward SE and then moved toward north. The bilateral rupture could explain some observed effects, toward N-NW and toward SE in terms of peak values and frequency content. With reference to the August 24th event, the Amatrice station, located at the south



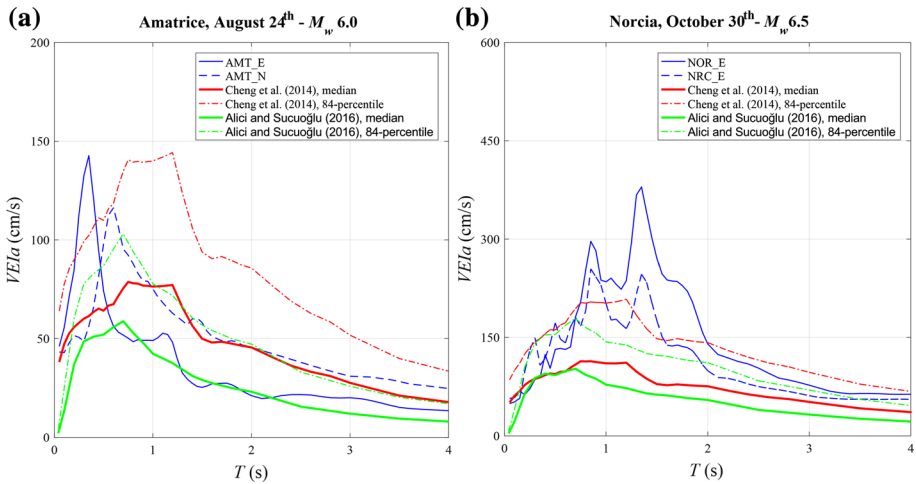


**Fig. 8** Comparison of the prediction of elastic input energy equivalent velocities (Cheng et al. 2014) with AMT\_E and AMT\_N components of the Amatrice recording station of August 24th (a) and with NOR\_E and NCR\_N components of the two Norcia recording stations of the October 30th (b). Input for calculation of these spectra are: distance=0.5 km,  $V_{s,30}$ =400 m/s, and  $M_w$  6.0 (a) and  $M_w$  6.5 (b)

of the surface projection of the fault (Fig. 1), shows the maximum energy at periods of 0.35 s ( $10,179 \text{ cm}^2/\text{s}^2$ ) and 0.60 s ( $6747 \text{ cm}^2/\text{s}^2$ ) for the EW and NS components, respectively (Fig. 6b). These peaks are then followed by a uniform energy demand decrease with increasing periods, without any other secondary peaks that could suggest the presence of long duration pulses (Mollaioli and Bosi 2012). In fact, the AMT ground motion shows evidence of polarization in the fault-normal direction only at short periods ( $<0.80$  s). On the contrary, for the same event, the NRC motion (EW component) shows higher amplitudes in the energy spectrum at 0.25, 0.75, and 1.25 s, with comparable values around  $5600 \text{ cm}^2/\text{s}^2$  (Fig. 6b). AMT has a shorter duration compared to NRC and a higher energy content. The length of the NRC recording and the presence of secondary peaks at longer periods could be ascribed also to possible site and soil effects (Lanzano et al. 2016).

In order to check the possibility of forward directivity effects, firstly, the energy demands have been evaluated for multiple orientations, by projecting the two components according to different angles. It was found, for the near fault records of the August 24th event, neither polarization of the ground motions in the fault-normal direction nor the presence of appreciable pulse-like characteristics of the signals in terms of maximum energy demands in the EW direction, except for AMT station. However, using the techniques mentioned in Sect. 4.2 (Baker 2007; Zhai et al. 2013; Dragomiretskiy and Zosso 2014), the presence of pulses has been identified for the stations of NOR, NRC and AMT, as shown by Luzi et al. (2017) and Iervolino et al. (2017). As already underlined, it is more difficult to identify the presence of pulses in energy spectra when, due to soil amplification, there are several peaks, as in the case of NOR and NRC stations.

The October 26th events ( $M_w$  5.4 and 5.9), occurred nearby Castelsantangelo sul Nera, activated another sector located to the NW of the first event, with a rupture propagation toward the N, i.e. toward Colfiorito, that released a moderate amount of seismic moment (Pischiutta et al. 2016). For the CMI records the maximum energy demand was discovered for the EW direction, nearly along the direction normal to the fault. For this station, at least

two of the methods mentioned above indicated the pulse-like characteristic of the motion. The periods related to the maximum energy demand correspond approximately to the periods of the pulses shown in Fig. 10, where the velocity time histories are reported together with the pulses extracted according to Baker (2007), even though the Baker's pulse indicator did not detect a pulse-like signal for the  $M_w$  5.9 event.

Directivity effects were observed for the  $M_w$  6.5 event of October 30th, as shown in Fig. 9. The maximum energy demand ( $E_{I,max} = 72,178 \text{ cm}^2/\text{s}^2$ ) is obtained for the NOR station (no. 4 in Fig. 1) approximately along the fault-normal direction. A pulse-like motion is recognised in this direction by using the variational mode decomposition technique (Dragomiretskiy and Zosso 2014). The NRC station (no. 2 in Fig. 1) presents its maximum energy demand nearly along the EW direction. In this case the variational approach indicated a pulse-like motion as well. According to this approach, the records are decomposed into different modes. Each extracted modes has been then analysed according to Baker's method, founding a score of the pulse indicator equal to 1 for the first mode, which indicates a pulse-like signal. It is useful to mention that Baker's method did not directly identify NOR and NRC original records as pulse-like for the October 30th event, probably due to the fact that the pulse is a late arrival one and it is therefore disregarded. Finally, records of the T1201 station (no. 6 in Fig. 1) reach maximum values approximately along the NS direction (Fig. 9), as identified by Luzi et al. (2017) and Iervolino et al. (2017). Other records with lower velocities were not considered for these analyses.

Near fault and directivity pulses, as those highlighted in Fig. 10, should be taken into account by current codes. As a matter of fact, even if the effects of moderate to large earthquakes in the near fault area are known, only some seismic codes have considered them in their provisions (Somerville et al. 1997; Iervolino and Cornell 2008; Almufti et al. 2015). It is important to underline that when the effects of forward directivity and pulse-like ground motions are not included in the building fragility curves, the probability of collapse can be significantly underestimated (Champion and Liel 2012). The last two versions of the Italian building code (DMI 2008; DMIT 2018) do not consider near fault effects

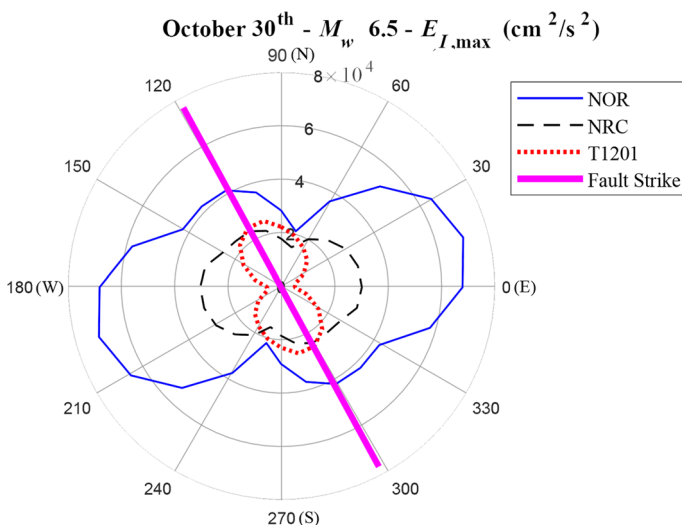
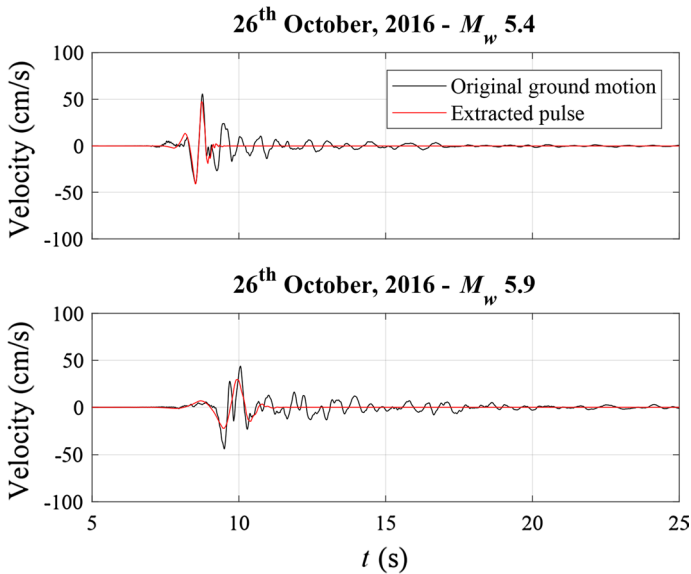


Fig. 9 Plot of maximum energy demand for different orientations



**Fig. 10** Velocity time histories and pulses extracted according to Baker (2007) for the October 26th events, CMI records

in the seismic design of structures, even though such effects were observed after Italian medium-magnitude earthquakes (Grimaz and Malisan 2014). Moreover, near fault effects are usually considered in seismic codes only for earthquakes with magnitude greater than 6.5. Indication of near-fault effects and presence of pulses in the recorded ground motions have been observed also after seismic events with lower magnitudes, such as the  $M_w$  6.3 L'Aquila earthquake (Chioccarelli and Iervolino 2010).

Finally, the seismic behaviour of structures subject to pulse-like ground motions is still a matter of studies (Rodriguez-Marek and Bray 2006; Baker 2007; Shahi and Baker 2011; Quaranta and Mollaioli 2018), and further research is needed to define appropriate intensity measures capable to characterize the presence of pulses and their damage potential in forward directivity ground motions (Mollaioli et al. 2006; Mollaioli and Bosi 2012; Chang et al. 2016).

## 6 Displacement spectra

Elastic displacement spectra,  $S_d$ , have been calculated for accelerograms with  $D_f \leq 40$  km. Considering the event of August 24th, the largest spectral displacements are obtained in Amatrice and Norcia stations, where a peak value of about 15 cm is reached. No significant difference between the NS and EW components is noted in Norcia, whereas a prevalence of the NS component is evident in Amatrice. For the event of October 26th spectral displacements are generally lower than 10 cm, with the exception of the EW component of the accelerogram recorded in Campi, where a peak value of 14 cm is attained. Displacements estimated for the event of October 30th are considerably larger, consistently with the larger magnitude. Values as high as 45 cm are estimated in Norcia.

To investigate the influence of the source distance, displacement spectra have been grouped according to the distance between the recording station and the surface projection of the fault,  $D_f$ . Four distance intervals are considered, namely  $D_f \leq 5$  km;  $5 < D_f \leq 12$  km,  $12 < D_f \leq 30$  km and  $D_f > 30$  km. As expected, the attenuation of the displacement demand with increasing distance is remarkable. Regarding the events occurred on August 24th ( $M_w$  6.0) and October 30th ( $M_w$  6.5) displacement spectra are shown in Fig. 11 for records having  $D_f \leq 5$  km. In the same figures there are presented: the average spectra, the average plus and minus one standard deviation spectra, the displacement design spectra proposed by Decanini et al. (2003) as well as the displacement response spectra based on the prediction equations by Cauzzi and Faccioli (2008). The Decanini et al. design spectra are bilinear curves defined so as to approach the mean plus a standard deviation of a set of about 300 accelerograms. They are defined for two intervals of magnitudes, i.e. 5.4–6.2 and 6.5–7.1, for different ranges of  $D_f$  and different soil types, namely S1, S2 and S3, roughly corresponding to A, B–C and D soils, respectively. The spectra based on the prediction equations proposed by Cauzzi and Faccioli (2008), which are derived by employing a very large data set (more than 1150 records), are continuous functions with coefficients depending on the magnitude of the event, focal distance and soil type (A, B, C, D). The error term is explicitly considered in this model and it is used herein for the estimation of the mean  $\pm$  one standard deviation spectra. Figure 11a highlights that the Decanini et al. design spectra overestimate the displacement demand of the August 24th event, whereas an opposite result is obtained with the Cauzzi and Faccioli spectra. For the October 30th event, in some cases the displacement demand in the near fault ( $D_f \leq 5$  km) is underestimated by both predicting models (Fig. 11b).

In Fig. 12, displacement spectra of Amatrice (AMT station) and Norcia (NRC and NOR stations) are compared with the Italian code design spectra for 475, 975 and 2475 years return periods (DMIT 2018). Considering the October 30th event, the displacement demand in Norcia exceeds the code spectra (Fig. 12b), especially in the short to medium

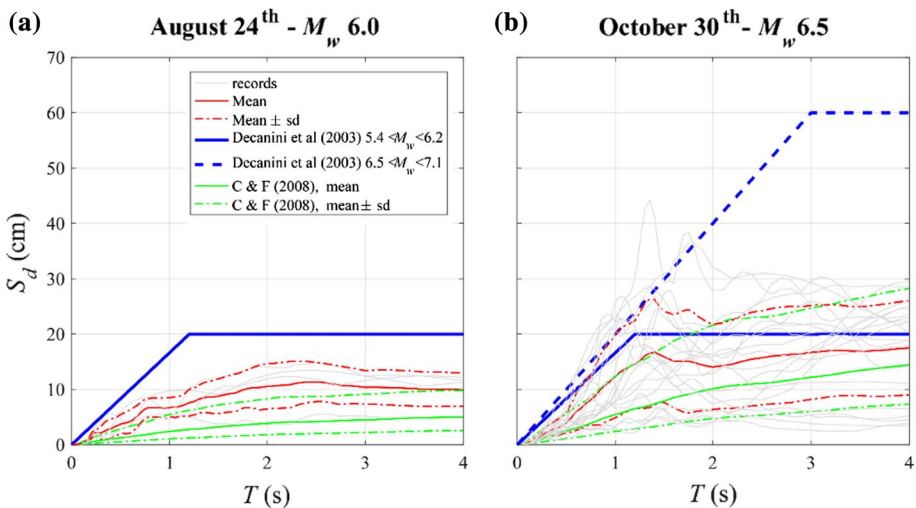


**Fig. 11** Displacement spectra for a distance from the fault  $D_f \leq 5$  km: **a** August 24th and **b** October 30th events. Comparison to design spectra proposed by Decanini et al. (2003), for an intermediate soil (S2), and the spectra based on the prediction equations by Cauzzi and Faccioli (2008)

period range, up to about 2 s. A better agreement is obtained in other cases (e.g. see Fig. 12a), where the displacement demand is generally near or below the design spectra.

Finally, in Fig. 13, displacement spectra of the Central Italy earthquakes are compared to those of three previous Italian seismic events: 1997 Umbria-Marche (Decanini et al. 2000), 2009 L’Aquila (Decanini et al. 2012) and 2012 Emilia (de Nardis et al. 2014). The shaking that occurred in Central Italy on October 30th is comparable or more severe to that in L’Aquila and in Emilia for periods less than about 1.5 s. For longer periods, the NS component of MRN29 (Mirandola station, May 29th, 2012 Emilia earthquake) exhibits a larger displacement demand. In Amatrice, the displacement demand was generally lower than that recorded during the other earthquakes. However, the sequence of events contributed to increase the damage, as frequent during Italian seismic swarms (Casolo 2017). An example is reported in Fig. 14, where the same column of a reinforced concrete building in Amatrice is shown after the August 24th event (Fig. 14a) and after the October 30th event (Fig. 14b). A significant increase of the longitudinal reinforcement buckling and of the concrete damage can be noticed, as well as the stirrup failure.

### 7 Rocking spectra

The Central Italy earthquake sequence has affected many unreinforced masonry and monumental structures. When connections are not effective or height/thickness ratios are large, these type of buildings may suffer out-of-plane mechanisms and undergo rocking (Penna 2015; Abrams et al. 2017; Marotta et al. 2017a). Therefore, in addition to the other response spectra presented herein, and considering the presence of rather slender bell gables that survived repeated shaking (Fig. 15a, b), it is worth calculating rocking spectra.

A rocking spectrum is a plot of the maximum angular displacement (Makris and Konstantinidis 2003) undergone by a rigid body rotating about its two base corners (Housner 1963). The body is described by its geometry ( $h/b$  ratio, Fig. 15c) and frequency parameter  $p$ , which is a function of mass,  $m$ , and shape of the body ( $p^2 = m g R/I_O$ , with  $I_O$  = polar moment of inertia about the base corner,  $g$  = gravity acceleration,  $R$  shown in Fig. 15c). In

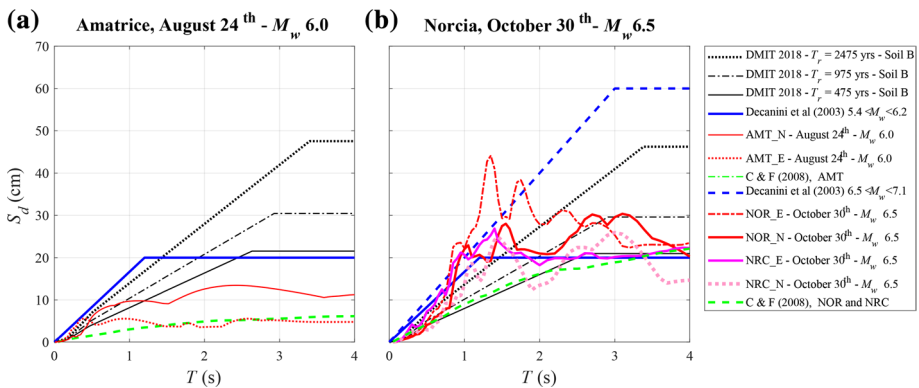


**Fig. 12** Comparison between records and code displacement spectra: **a** Amatrice, August 24th event and **b** Norcia, October 30th event. Black lines refer to code design spectra (DMIT 2018), estimated for 475, 975 and 2475 years return periods. Red lines are used for design spectra proposed by Decanini et al. (2003), estimated for different magnitude ranges, blue lines represent the spectra based on the prediction equations by Cauzzi and Faccioli (2008)

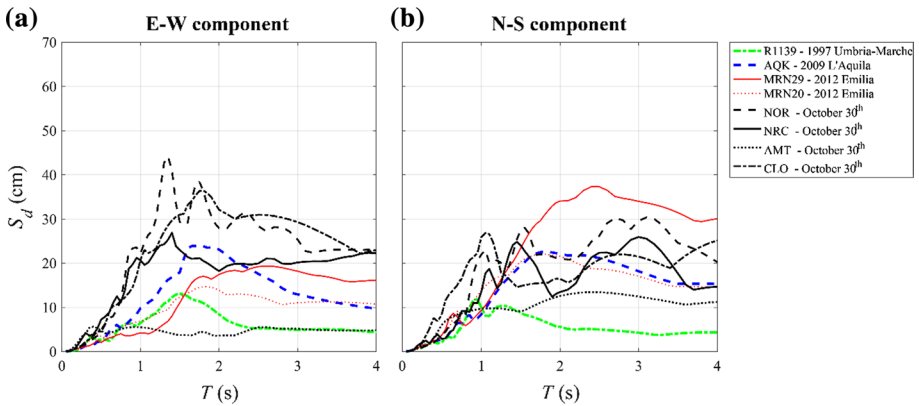


**Fig. 13** Displacement spectra, comparison with other Italian earthquakes: **a** E–W component and **b** N–S component. Spectra of the 2016 earthquake in Central Italy (black lines) are related to the October 30th event

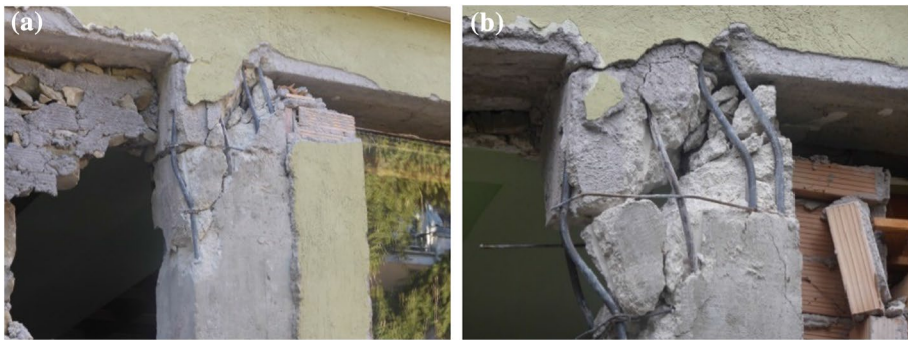


**Fig. 14** Progressive damage to a reinforced concrete building in Amatrice: **a** after the August 24th event and **b** after the October 30th event

the case of rectangular vertical cross section  $p^2 = 3g/4R$  and, consequently, the smaller the size the larger  $p$ . The rocking body can be assumed to be representative of the behaviour of a number of artefacts, such as equipment, tombstones, parapet walls, crenellations, isolated slender constructions, and so on (Lagomarsino 2015), while its extension to multiple-body kinematic chains is only indirect (Sorrentino et al. 2017a). Because unreinforced masonry elements are the most relevant here, Housner model has been fine tuned according to experimental evidence, involving a three branch restoring moment—angular displacement law and an appropriate energy damping (Al Shawa et al. 2012).

In this study, the following ranges of values have been considered:  $2\pi/p = 0–6$  s, corresponding to homogeneous bodies up to more than 13 m tall;  $h/b = 4–10$ . The response of a rocking body can be affected by marked dispersion of output results for small variations of input data. Hence, for each combination of  $2\pi/p$  and  $h/b$  values, 25 non-linear time-history analyses have been carried out, by multiplying each record by 25 amplitude scale factors belonging to a Gaussian distribution with unity mean and 0.03 standard deviation. Since, once overturned, the angular displacement increases without bound, it is not correct to

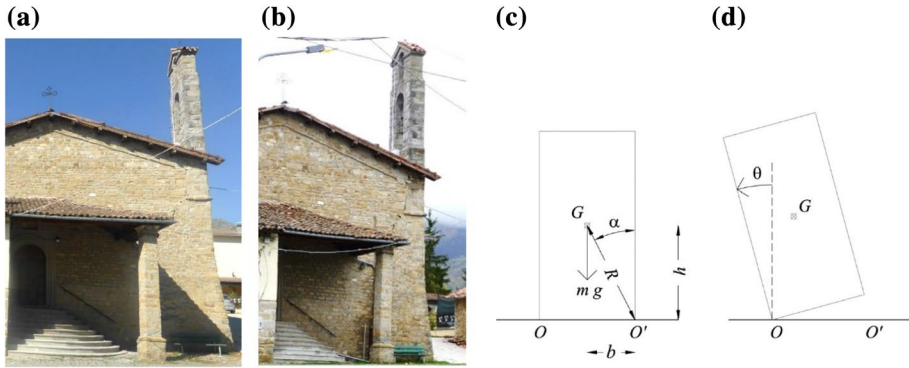


**Fig. 15** Unreinforced masonry bell gable of San Cipriano in Amatrice. **a** After the August 24th event and **b** after the October 30th event. Model of a rocking rigid body: **c** parameters describing the model and **d** angular displacement

compute an average value of maximum rotations of dynamic analyses and a median value is considered hereinafter;  $\max(|\theta|)$  characterizes the rotation demand (Fig. 15d), whereas  $\alpha$  is the corresponding capacity (Fig. 15c). A ratio  $\max(|\theta|/\alpha) = 1$  involves instability under gravity.

Rocking spectra have been computed for the accelerograms recorded in Amatrice and in Norcia on August 24th,  $M_w$  6.0 (Fig. 16a–d) and on October 30th,  $M_w$  6.5 (Fig. 16e–h). An increasing abscissa involves an increasing size of the body, while an increasing ordinate involves a more severe response. As usual, for a given size of the body and apart from outliers, the smaller the height/thickness ratio the smaller the response. Rocking bodies show a dynamic reserve of stability, so rocking initiation does not necessarily imply overturning (Mauro et al. 2015). Moreover, they highlight a so-defined “scale effect”, the larger the size (i.e. the smaller  $p$ ) the smaller the response (Housner 1963). These phenomena are evident in Fig. 16 (first row), where it is possible to observe that in Amatrice, despite the dramatic difference in PGA, the two horizontal components involve similar responses, whereas in Norcia there is a slightly more marked difference in rocking. The comparison between the two locations shows a more severe response in Norcia. The October 30th event involves a similar level of displacement demand in Amatrice and a significant increase in Norcia Fig. 16 (second row). In the case of the East–West component of Amatrice, for a height/thickness ratio equal to 10 an increase of the response can be observed. This phenomenon is visible already for  $h/b = 9$  (not shown for the sake of conciseness), and is related to a lower level of ground motion acceleration able to trigger a significant rotation at about 14 s from the beginning of the ground motion time history, thus making the rotated wall vulnerable to a pulse following about 3 s later. Squatter walls ( $h/b < 9$ ) are not displaced enough to suffer from this later pulse.

For comparison purposes, the spectra of the Central Italy earthquakes are compared to those of the 2009 L’Aquila event, and of the 2012 Emilia earthquake. Records can be compared in terms of cumulative frequency of overturnings, i.e. the number of overturnings divided by the number of analyses for all the aspect ratios. From Table 5 it is apparent that the EW component of the October 30th record in Norcia is comparable or more severe than that in L’Aquila and in Mirandola. In Amatrice, expected rocking response has been less severe, thus contributing to explain why slender bell gables survived (Fig. 15a,

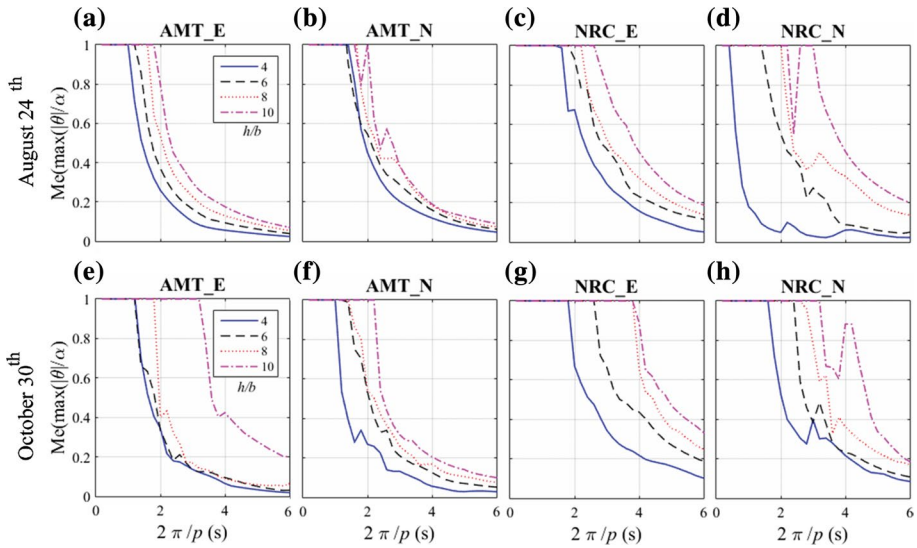


**Fig. 16** Rocking spectra. First row: August 24th event. Second row: October 30th event. **a, b, e, f** Amatrice station records and **c, d, g, h** Norcia (NRC) station records

b). However, rocking response is possible if masonry fragmentation is prevented, thanks to appropriate bond or adequate mortar (Liberatore et al. 2016), but such fragmentation occurred in a large proportion of the unreinforced masonry buildings in and around Amatrice (Sorrentino et al. 2017b).

### 8 Conclusions

Four regions of Central Italy (Lazio, Umbria, Abruzzo and Marche) were strongly affected by the seismic sequence started at the end of August, 2016. In many villages of the affected area, masonry constructions, reinforced concrete buildings and churches were severely damaged. Buildings vulnerability was not the same in the whole area also due to the different seismic classification. Some municipalities were not classified as seismic prone until 1981 or 1983 (e.g. Arquata del Tronto) or were originally attributed to seismic zone with lower seismicity compared to the current one (e.g. Accumoli and Amatrice). In the past, changes to the seismic zonation were based on earthquake occurrences. Occurrences of

**Table 5** Cumulative frequency of overturning of the rocking spectra for horizontal component

Events station	Central Italy August 24th		Central Italy October 30th		2009 L'Aquila AQK	2012 Emilia MRN (May 20th)
	AMT	NRC	AMT	NRC		
EW component	0.23	0.32	0.29	0.48	0.45	0.33
NS component	0.22	0.26	0.24	0.40	0.47	0.40

0, no overturning; 1, 100% overturning



earthquakes also affected the buildings typology and resistance to seismic loads. For example, after the earthquake of 1859, buildings in Norcia were reconstructed limiting the number of storeys and adopting specific earthquake resistant details, whereas after the earthquakes of 1979 and 1997, strengthening interventions were adopted for masonry buildings. Different vulnerabilities may explain, to a certain extent, the seismic response surveyed in the area. In addition, structural response was noticeably affected by the characteristics of ground motion. In this study, the damage potential of the accelerograms recorded during the strongest events of the sequence was assessed. Different intensity measures related to the ground motion records have been calculated, elastic spectral demands, in terms of pseudo-accelerations, energies (equivalent velocity), displacements and rocking rotations have been estimated and discussed. Whenever appropriate, the spectral demands are compared with those of Italian seismic codes and previous Italian earthquakes. The main inferences of the study can be summarised as follows.

- The intensity measures related to velocities, such as the Incremental Velocity and Housner Intensity, provided interesting information. Particularly, for the October 30th event, the highest values ever recorded in Italy were attained in Norcia, Domo and Castelluccio. Such large values denote that the acceleration spectrum is shifted towards low frequencies and it is also an index of the presence of long duration pulses due to directivity or soil amplification effects. The strong correlation between damage to churches and Housner Intensity, as well as the sensitivity of local mechanisms to long period pulses, may contribute to explain the extensive damage to churches in Norcia, but additional specific analyses are necessary. Damage in very stiff shear walls and in rubble masonry with poor mortar can be related, instead, to the effect of high frequencies, which were highlighted by the comparison between Peak Ground Acceleration and Effective Peak Acceleration values.
- Pseudo-acceleration spectra showed high demands in the low periods range (up to 0.5 s) for all the events, with the exception of that occurred on October 30th, which exhibits secondary peaks at longer periods. This circumstance can be associated with the severe damage to ordinary unreinforced masonry buildings and to low-rise infilled reinforced concrete buildings observed in Amatrice after the August 24th event, whereas damage was somewhat more limited on taller structures. The vertical component of the ground motion was also extremely large in the near fault, especially during the October 30th event.
- The comparison between the acceleration spectra and the design code spectra highlighted that, in some cases (e.g. in Amatrice during the August 24th event) the records' spectra largely exceeded the 2475 years return period design spectrum in the plateau range of periods. For the October 30th event, the design spectra are exceeded also for periods between about 0.7 and 1.5 s, due to the presence of the above mentioned secondary peaks.
- The possibility of forward directivity effects, suggested by the high values of the velocity related intensity measures and by the presence of acceleration peaks at periods greater than 0.7 s, has been investigated. To this aim, the energy demands have been calculated along different directions. Moreover, three different approaches have been used to detect the presence of long duration pulses. Directivity effects were observed for the event of October 30th. In this case, the maximum energy demand is obtained for Norcia stations (NOR and NRC) approximately along the fault-normal direction, where a pulse-like motion is also identified by using the variational decomposition method. For the near fault records of the August 24th and October 26th events, neither polariza-

tion of the ground motions in the fault-normal direction nor the presence of significant pulse-like characteristics of the signals in terms of maximum energy demands were found, except for Amatrice station (AMT). However, using Baker (2007) and Dragomiretskiy and Zosso (2014) methods, the presence of pulses was found also for Norcia (NOR and NRC) and CMI stations.

- Elastic displacement spectra showed moderate values, with the exception of those obtained for the October 30th event, where a peak value of 45 cm was obtained. Considering usual configurations of infilled reinforced concrete frame buildings, this value can be associated to a high level of damage or to a near collapse condition depending on whether the building is designed according to seismic criteria or not.
- Rocking spectra have been computed for the most severe accelerograms recorded in Amatrice and in Norcia on August 24th and on October 30th. The comparison between the two locations shows a more severe response in Norcia. This observation can contribute to explain the survival of rather slender bell gables in Amatrice.

**Acknowledgements** The financial support of the Ministry of the Instruction, University and Research of Italy (MIUR) is gratefully acknowledged. This work has been partially carried out under the program “Dipartimento di Protezione Civile—Consorzio Reluis 2017. The contribution of the anonymous reviewers is acknowledged.

## References

- Abrams DP, AlShawa O, Lourenço PB, Sorrentino L (2017) Out-of-plane seismic response of unreinforced masonry walls: conceptual discussion, research needs, and modeling issues. *Int J Archit Herit* 11:22–30. <https://doi.org/10.1080/15583058.2016.1238977>
- Al Shawa O, de Felice G, Mauro A, Sorrentino L (2012) Out-of-plane seismic behaviour of rocking masonry walls. *Earthq Eng Struct Dyn* 41:949–968. <https://doi.org/10.1002/eqe.1168>
- Almufiti I, Motamed R, Grant DN, Willford M (2015) Incorporation of velocity pulses in design ground motions for response history analysis using a probabilistic framework. *Earthq Spectra* 31:1647–1666. <https://doi.org/10.1193/032113EQS072M>
- Anderson JC, Bertero VV (1987) Uncertainties in establishing design earthquakes. *J Struct Eng (United States)* 113:1709–1724. [https://doi.org/10.1061/\(ASCE\)0733-9445\(1987\)113:8\(1709\)](https://doi.org/10.1061/(ASCE)0733-9445(1987)113:8(1709))
- Arias A (1970) A measure of earthquake intensity. In: Hansen RJ (ed) *Seismic design for nuclear power plants*. MIT Press, Cambridge, pp 438–483
- ATC (1978) Applied technology council. Tentative provisions for the development of seismic regulations for buildings, Special publication 510. US National Bureau of Standards
- Baker JW (2007) Quantitative classification of near-fault ground motions using wavelet analysis. *Bull Seismol Soc Am* 97:1486–1501. <https://doi.org/10.1785/0120060255>
- Bindi D, Luzi L, Parolai S et al (2011) Site effects observed in alluvial basins: the case of Norcia (Central Italy). *Bull Earthq Eng* 9:1941–1959. <https://doi.org/10.1007/s10518-011-9273-3>
- Borri A, Calderini C, Carocci CF et al (2017) Damage to churches in the 2016 central Italy earthquakes. *Bull Earthq Eng* 16:1399–1423
- Cabañas L, Benito B, Herráiz M (1997) An approach to the measurement of the potential structural damage of earthquake ground motions. *Earthq Eng Struct Dyn* 26:79–92. [https://doi.org/10.1002/\(SICI\)1096-9845\(199701\)26:1%3c79:AID-EQE624%3e3.0.CO;2-Y](https://doi.org/10.1002/(SICI)1096-9845(199701)26:1%3c79:AID-EQE624%3e3.0.CO;2-Y)
- Casolo S (2017) A numerical study on the cumulative out-of-plane damage to church masonry façades due to a sequence of strong ground motions. *Earthq Eng Struct Dyn* 46:2717–2737. <https://doi.org/10.1002/eqe.2927>
- Cauzzi C, Faccioli E (2008) Broadband (0.05 to 20 s) prediction of displacement response spectra based on worldwide digital records. *J Seismol* 12:453–475. <https://doi.org/10.1007/s10950-008-9098-y>
- Champion C, Liel A (2012) The effect of near-fault directivity on building seismic collapse risk. *Earthq Eng Struct Dyn* 41:1391–1409. <https://doi.org/10.1002/eqe.1188>

- Chang Z, Sun X, Zhai C et al (2016) An improved energy-based approach for selecting pulse-like ground motions. *Earthq Eng Struct Dyn* 45:2405–2411. <https://doi.org/10.1002/eqe.2758>
- Cheng Y, Lucchini A, Mollaioli F (2014) Proposal of new ground-motion prediction equations for elastic input energy spectra. *Earthq Struct* 7:485–510. <https://doi.org/10.12989/eas.2014.7.4.485>
- Chiaraluce L, Di Stefano R, Tinti E et al (2017) The 2016 Central Italy seismic sequence: a first look at the mainshocks, aftershocks, and source models. *Seismol Res Lett* 88:1–15
- Chioccarelli E, Iervolino I (2010) Near-source seismic demand and pulse-like records: a discussion for L'Aquila earthquake. *Earthq Eng Struct Dyn* 39:1039–1062. <https://doi.org/10.1002/eqe.987>
- Crowley H, Stucchi M, Meletti C et al (2009) Revisiting Italian design code spectra following the L'Aquila earthquake. *Progett Sismica* 1:73–81
- Curti E, Podestá S, Scandolo L (2012) Simplified mechanical model for the seismic vulnerability evaluation of bellfries. *Int J Archit Herit* 6:605–625. <https://doi.org/10.1080/15583058.2011.594932>
- de Nardis R, Filippi L, Costa G et al (2014) Strong motion recorded during the Emilia 2012 thrust earthquakes (Northern Italy): a comprehensive analysis. *Bull Earthq Eng*. <https://doi.org/10.1007/s10518-014-9614-0>
- Decanini LD, Mollaioli F (1998) Formulation of elastic earthquake input energy spectra. *Earthq Eng Struct Dyn* 27:1503–1522. [https://doi.org/10.1002/\(SICI\)1096-9845\(199812\)27:12%3c1503:AID-EQE797%3e3.0.CO;2-A](https://doi.org/10.1002/(SICI)1096-9845(199812)27:12%3c1503:AID-EQE797%3e3.0.CO;2-A)
- Decanini L, Gavarini C, Mollaioli F (2000) Some remarks on the Umbria-Marche Earthquakes of 1997. *Eur Earthq Eng* 3:18–48
- Decanini LD, Liberatore L, Mollaioli F (2002) Response of bare and infilled RC frames under the effect of horizontal and vertical seismic excitation. In: Proceedings of 12th European conference on earthquake engineering, London, 9–13 September
- Decanini LD, Liberatore L, Mollaioli F (2003) Characterization of displacement demand for elastic and inelastic SDOF systems. *Soil Dyn Earthq Eng*. [https://doi.org/10.1016/S0267-7261\(03\)00062-9](https://doi.org/10.1016/S0267-7261(03)00062-9)
- Decanini LD, Liberatore L, Mollaioli F (2012) Damage potential of the 2009 L'Aquila, Italy, earthquake. *J Earthq Tsunami* 6:1250032. <https://doi.org/10.1142/S1793431112500327>
- DMI (2008) Decreto del Ministro delle Infrastrutture 14 gennaio 2008. Approvazione delle nuove norme tecniche per le costruzioni. *Gazzetta Ufficiale della Repubblica Italiana*, n. 29 del 4 febbraio 2008, Supplemento Ordinario n. 30
- DMIT (2018) Decreto del Ministro delle Infrastrutture e dei Trasporti 17 gennaio 2018. Aggiornamento delle “Norme tecniche per le costruzioni”. *Gazzetta Ufficiale della Repubblica Italiana*, n. 42 del 20 febbraio 2018, Supplemento Ordinario n. 8
- DMLP (1975) Decreto del Ministro dei Lavori Pubblici n. 39 del 3 marzo 1975. Approvazione delle Norme Tecniche per le Costruzioni in Zone Sismiche. *Gazzetta Ufficiale della Repubblica Italiana*, 8 aprile 1975, n. 93
- DMLP (1996) Decreto del Ministro dei Lavori Pubblici del 16 gennaio 1996. Norme Tecniche per le Costruzioni in Zone Sismiche. *Gazzetta Ufficiale della Repubblica Italiana*, 5 febbraio 1996, n. 19
- Dragomiretskiy K, Zosso D (2014) Variational mode decomposition. *IEEE Trans Signal Process* 62:531–544. <https://doi.org/10.1109/TSP.2013.2288675>
- Fumagalli F, Liberatore D, Monti G, Sorrentino L (2017) Building features of Accumoli and Amatrice in a pre-earthquake survey. In: Proceedings of the 17th Italian National conference on earthquake engineering, Pistoia, 17–21 September, pp SG03.45–SG03.54
- Grimaz S, Malisan P (2014) Near field domain effects and their consideration in the international and Italian seismic codes. *Boll di Geofis Teor ed Appl* 55:717–738. <https://doi.org/10.4430/bgta0130>
- Housner GW (1952) Spectrum intensities of strong motion earthquakes. In: Proceedings of the symposium of earthquake and blast effects on structures, EERI, Los Angeles, CA, pp 21–36
- Housner GW (1963) The behavior of inverted pendulum structures during earthquakes. *Bull Seismol Soc Am* 53:403–417. <https://doi.org/10.1017/CBO9781107415324.004>
- Iervolino I (2013) Probabilities and fallacies: why hazard maps cannot be validated by individual earthquakes. *Earthq Spectra* 29:1125–1136
- Iervolino I, Cornell CA (2008) Probability of occurrence of velocity pulses in near-source ground motions. *Bull Seismol Soc Am* 98:2262–2277. <https://doi.org/10.1785/0120080033>
- Iervolino I, Baltzopoulos G, Chioccarelli E, Suzuki A (2017) Seismic actions on structures in the near-source region of the 2016 central Italy sequence. *Bull Earthq Eng*. <https://doi.org/10.1007/s10518-017-0295-3>
- Lagomarsino S (2015) Seismic assessment of rocking masonry structures. *Bull Earthq Eng* 13:97–128. <https://doi.org/10.1007/s10518-014-9609-x>
- Lanzano G, Luzi L, Pacor F et al (2016) Preliminary analysis of the accelerometric recordings of the August 24th, 2016 Mw 6.0 amatrice earthquake. *Ann Geophys* 59:1–7. <https://doi.org/10.4401/ag-7201>

- Liberatore L, Sorrentino L, Liberatore D, Decanini LD (2013) Failure of industrial structures induced by the Emilia (Italy) 2012 earthquakes. *Eng Fail Anal* 34:629–647. <https://doi.org/10.1016/j.engfailanal.2013.02.009>
- Liberatore D, Masini N, Sorrentino L et al (2016) Static penetration test for historical masonry mortar. *Constr Build Mater*. <https://doi.org/10.1016/j.conbuildmat.2016.07.097>
- Luzi L, Puglia R, Russo E, WG5 O (2016) Engineering strong motion database, version 1.0. In: *Obs. Res. Facil. Eur. Seismol*
- Luzi L, Pacor F, Puglia R et al (2017) The Central Italy seismic sequence between August and December 2016: analysis of strong-motion observations. *Seismol Res Lett* 88:1219–1231. <https://doi.org/10.1785/0220170037>
- Makris N, Konstantinidis D (2003) The rocking spectrum and the limitations of practical design methodologies. *Earthq Eng Struct Dyn* 32:265–289. <https://doi.org/10.1002/eqe.223>
- Marotta A, Sorrentino L, Liberatore D, Ingham JM (2017a) Vulnerability assessment of unreinforced masonry churches following the 2010–2011 Canterbury (New Zealand) earthquake sequence. *J Earthq Eng* 21:912–934. <https://doi.org/10.1080/13632469.2016.1206761>
- Marotta A, Sorrentino L, Liberatore D, Ingham JM (2017b) Seismic risk assessment of New Zealand unreinforced masonry churches using statistical procedures. *Int J Archit Herit*. <https://doi.org/10.1080/15583058.2017.1323242>
- Mauro A, de Felice G, DeJong MJ (2015) The relative dynamic resilience of masonry collapse mechanisms. *Eng Struct* 85:182–194. <https://doi.org/10.1016/j.engstruct.2014.11.021>
- Mollaioli F, Bosi A (2012) Wavelet analysis for the characterization of forward-directivity pulse-like ground motions on energy basis. *Meccanica* 47:203–219. <https://doi.org/10.1007/s11012-011-9433-1>
- Mollaioli F, Bruno S, Decanini LD, Panza GF (2006) Characterization of the dynamic response of structures to damaging pulse-type near-fault ground motions. *Meccanica* 41:23–46. <https://doi.org/10.1007/s11012-005-7965-y>
- Mollaioli F, Bruno S, Decanini L, Saragoni R (2011) Correlations between energy and displacement demands for performance-based seismic engineering. *Pure Appl Geophys* 168:237–259. <https://doi.org/10.1007/s00024-010-0118-9>
- Mollaioli F, Liberatore L, Lucchini A (2014) Displacement damping modification factors for pulse-like and ordinary records. *Eng Struct* 78:17–27. <https://doi.org/10.1016/j.engstruct.2014.07.046>
- OPCM (2003) Ordinanza del Presidente del Consiglio dei Ministri n. 3274 del 20 marzo 2003. *Primi elementi in materia di criteri generali per la classificazione sismica del territorio nazionale e di normative tecniche per le costruzioni in zona sismica*. Gazzetta Ufficiale, 8 maggio 2003, n. 105
- Penna A (2015) Seismic assessment of existing and strengthened stone-masonry buildings: critical issues and possible strategies. *Bull Earthq Eng* 13:1051–1071. <https://doi.org/10.1007/s10518-014-9659-0>
- Pischiutta M, Akinci A, Malagnini L, Herrero A (2016) Characteristics of the strong ground motion from the 24th August 2016 Amatrice earthquake. *Ann Geophys* 59:1–8. <https://doi.org/10.4401/AG-7219>
- Quaranta G, Mollaioli F (2018) On the use of the equivalent linearization for bilinear oscillators under pulse-like ground motion. *Eng Struct* 160:395–407. <https://doi.org/10.1016/j.engstruct.2018.01.055>
- Rodriguez-Marek A, Bray JD (2006) Seismic site response for near-fault forward directivity ground motions. *J Geotech Geoenviron Eng* 132:1611–1620. [https://doi.org/10.1061/\(ASCE\)1090-0241\(2006\)132:12\(1611\)](https://doi.org/10.1061/(ASCE)1090-0241(2006)132:12(1611))
- Shahi SK, Baker JW (2011) An empirically calibrated framework for including the effects of near-fault directivity in probabilistic seismic hazard analysis. *Bull Seismol Soc Am* 101:742–755. <https://doi.org/10.1785/0120100090>
- Shrestha B (2009) Vertical ground motion and its effect on engineering structures: a state-of-the-art review. *International seminar on hazard management for sustainable development*. Nepal, Kathmandu, pp 190–202
- Sisti R, Di Ludovico M, Borri A, Prota A (2018) Damage assessment and the effectiveness of prevention: the response of ordinary unreinforced masonry buildings in Norcia during the Central Italy 2016–2017 seismic sequence. *Bull Earthq Eng*. <https://doi.org/10.1007/s10518-018-0448-z>
- Somerville PG, Smith NF, Graves RW, Abrahamson NA (1997) Modification of empirical strong ground motion attenuation relations to include the amplitude and duration effects of rupture directivity. *Seismol Res Lett* 68:199–222. <https://doi.org/10.1785/gssrl.68.1.199>
- Sorrentino L (2007) The early entrance of dynamics in earthquake engineering: Arturo Danusso's contribution. *ISET J Earthq Technol* 44:1–24
- Sorrentino L, Alshawa O, Liberatore D (2014) Observations of out-of-plane rocking in the oratory of san Giuseppe dei Minimi during the 2009 L'Aquila earthquake. *Appl Mech Mater* 621:101–106. <https://doi.org/10.4028/www.scientific.net/AMM.621.101>

- Sorrentino L, D'Ayala D, de Felice G et al (2017a) Review of out-of-plane seismic assessment techniques applied to existing masonry buildings. *Int J Archit Herit* 11:2–21. <https://doi.org/10.1080/15583058.2016.1237586>
- Sorrentino L, da Porto F, Magenes G, Penna A (2017b) Seismic behavior of ordinary masonry buildings during the 2016 Central Italy earthquakes. *Bull Earthq Eng*. <https://doi.org/10.1007/s10518-018-0370-4>
- Stucchi M, Meletti C, Montaldo V et al (2011) Seismic hazard assessment (2003–2009) for the Italian building code. *Bull Seismol Soc Am* 101:1885–1911. <https://doi.org/10.1785/0120100130>
- Tertulliani A, Azzaro R (2016) QUEST—Rilievo macrosismico per i terremoti nell'Italia centrale. Aggiornamento dopo le scosse del 26 e 30 ottobre 2016. Roma
- Tinti E, Scognamiglio L, Michelini A, Cocco M (2016) Slip heterogeneity and directivity of the ML 6.0, 2016, Amatrice earthquake estimated with rapid finite-fault inversion. *Geophys Res Lett* 43:10745–10752. <https://doi.org/10.1002/2016gl071263>
- Trifunac MD, Brady AG (1975) A study on the duration of strong earthquake ground motion. *Bull Seismol Soc Am* 65:581–626. [https://doi.org/10.1016/0148-9062\(76\)90487-3](https://doi.org/10.1016/0148-9062(76)90487-3)
- Uang C, Bertero V (1988) Implications of recorded earthquake ground motions on seismic design of building structures UCB/EERC-88/13. Report no. UCB/EERC-88/13
- Uang C, Bertero V (1990) Evaluation of seismic energy in structures. *Earthq Eng Struct Dyn* 3:519–559. <https://doi.org/10.1002/eqe.4290190108>
- Zhai C, Chang Z, Li S et al (2013) Quantitative identification of near-fault pulse-like ground motions based on energy. *Bull Seismol Soc Am* 103:2591–2603. <https://doi.org/10.1785/0120120320>